Development 137, 3719-3727 (2010) doi:10.1242/dev.050948

Disabled is a bona fide component of the Abl signaling network

Jeong K. Song[1], Ramakrishnan Kannan[1], Gunter Merdes[2], Jaskirat Singh[3], Marek Mlodzik[3] and Edward Giniger[1,*]

SUMMARY

Abl is an essential regulator of cell migration and morphogenesis in both vertebrates and invertebrates. It has long been speculated that the adaptor protein Disabled (Dab), which is a key regulator of neuronal migration in the vertebrate brain, might be a component of this signaling pathway, but this idea has been controversial. We now demonstrate that null mutations of *Drosophila Dab* result in phenotypes that mimic *Abl* mutant phenotypes, both in axon guidance and epithelial morphogenesis. The *Dab* mutant interacts genetically with mutations in *Abl*, and with mutations in the Abl accessory factors *trio* and *enabled* (*ena*). Genetic epistasis tests show that *Dab* functions upstream of *Abl* and *ena*, and, consistent with this, we show that Dab is required for the subcellular localization of these two proteins. We therefore infer that Dab is a bona fide component of the core Abl signaling pathway in *Drosophila*.

KEY WORDS: Disabled, Abl tyrosine kinase, Axon guidance, *Drosophila*, Epithelial morphogenesis

INTRODUCTION

The Abelson non-receptor tyrosine kinase (Abl) family has been implicated in a broad range of biological processes, such as oncogenesis, cell growth, adhesion, migration, neurite extension and growth cone motility (for a review, see Pendergast, 2002). For example, in *Drosophila*, *Abl* mutants often display guidance defects in CNS and motor axons (Wills et al., 1999a; Wills et al., 2002), as well as epithelial morphogenesis defects during syncytial pseudo-cleavage, cellularization and dorsal closure (Grevengoed et al., 2003; Grevengoed et al., 2001; Liebl et al., 2003). In mice, knockout of the Abl family kinase genes *Abl* (*Abl1* – Mouse Genome Informatics) and Abl-related gene (*Arg*; *Abl2* – Mouse Genome Informatics) (Gitai et al., 2003) causes defects in neural tube closure with cytoskeletal abnormalities such as disruption of the apical latticework and enrichment of actin at the basolateral surface (Koleske et al., 1998; Moresco et al., 2005). Abl acts at the center of the complex signaling network that executes neuronal morphogenesis (for a review, see Moresco and Koleske, 2003). For example, Abl interacts with axon guidance receptors such as Dcc, Robo, Lar and Notch (Bashaw et al., 2000; Crowner et al., 2003; Forsthoefel et al., 2005; Wills et al., 1999a), suggesting that a variety of guidance signals converge on the Abl signaling pathway and are integrated.

Abl acts in concert with conserved signaling components. Genetic experiments in fly identified one antagonist, Enabled (Ena) (Gertler et al., 1990) and three cooperating factors: Neurotactin (Nrt) (Liebl et al., 2003), Trio (Liebl et al., 2000) and Failed axon connections (Fax) (Hill et al., 1995). Nrt is a single-pass transmembrane protein involved in cell adhesion through the binding of its ligand, Amalgam (Fremion et al., 2000). Trio contains tandemly encoded guanine exchange factor (GEF) domains and activates the small GTPases Rac and Rho (Bateman et al., 2000; Briancon-Marjollet et al., 2008; Debant et al., 1996). Fax, a dominant enhancer of Abl (Hill et al., 1995), interacts in a dosage-sensitive manner with Trio (Liebl et al., 2000). Ena, a substrate of Abl (Gertler et al., 1995), facilitates actin polymerization at the barbed ends of actin filaments, in part by acting as an anti-capping protein (Barzik et al., 2005; Bear et al., 2002). Ena localization is disrupted by the absence of Abl, implying that Ena works downstream of Abl (Grevengoed et al., 2003). Recently, it has been shown that Abl interacting protein 1 (Abi1), first identified biochemically in mammalian cultured cells, acts as an antagonist of Abl signaling during axonogenesis through the modulation of F-actin distribution (Lin et al., 2009).

In addition to those molecules, Disabled (Dab) may also be a component of the Abl signaling pathway. Disabled is a tyrosine-phosphorylated adaptor protein (Gertler et al., 1993; Howell et al., 1997a; Le and Simon, 1998). It is a possible point of linkage of intracellular signaling to cell surface receptors. In *Drosophila*, it binds to the receptor Notch, and altering Dab levels modifies axon guidance phenotypes in *Notch* mutants (Le Gall et al., 2008; Le Gall and Giniger, 2004). In vertebrates, Dab is essential for neuronal migration and cortical layering during brain development (Howell et al., 1997b). Binding of the secreted protein reelin to its receptors, such as Vldlr and ApoE receptor 2, induces tyrosine phosphorylation of Dab1, a mouse homolog of Dab. Activated Dab1 then binds to Notch, which directly controls the radial migration of neurons to the appropriate layer of the developing neocortex (Hashimoto-Torii et al., 2008). When Disabled was first identified, it was thought to be a core component of the Abl signaling pathway (Hoffmann, 1991). In *Drosophila*, Dab is extensively co-expressed with Abl during development and modest overexpression of Dab suppresses the genetic interaction of *Abl* with *Nrt* and *fax* (Gertler et al., 1993; Hill et al., 1995; Liebl et al.,

[1]Axon Guidance and Neural Connectivity Unit, Basic Neuroscience Program, National Institute of Neurological Disorders and Stroke, National Institutes of Health, Bethesda, MD 20892, USA. [2]ETH Zürich, Department of Biosystems Science and Engineering, D-BSSE, Mattenstrasse 26, CH-4058 Basel, Switzerland. [3]Department of Developmental and Regenerative Biology, Mount Sinai School of Medicine, Annenberg Building 18-92, 1 Gustave L. Levy Place, New York, NY 10029, USA.

*Author for correspondence (ginigere@ninds.nih.gov)

Accepted 31 August 2010

2003). However, all the mutations originally ascribed to *Dab* were later found to be mutations of the nearby gene *Nrt*, and, as a result, the notion that Dab is linked to the Abl signaling pathway has become quite controversial (Liebl et al., 2003). To date, no mutations have been identified in *Drosophila Dab*.

We now show that Dab is a bona fide component of the Abl signaling pathway in *Drosophila*. We generate two independent null alleles of *Dab* and show that they produce motor axon patterning defects that are very similar to those of Abl pathway mutations. The *Dab* mutations interact synergistically with mutations in *Abl* and *trio,* and antagonistically to *ena*, demonstrating that *Dab* is a positive component of the pathway, and that, by genetic criteria, *Dab* functions upstream of *Abl* and *ena*. The *Dab* mutants, moreover, mimic non-neuronal phenotypes of *Abl* in epithelial morphogenesis such as syncytial pseudo-cleavage furrow formation, cellularization and dorsal closure. Finally, we show that Dab is required for proper subcellular distribution of Abl in those epithelia and in the retinal neuroepithelium, confirming its role as an upstream component of the Abl signaling module.

MATERIALS AND METHODS

Genetics

Dab^1 and Dab^2 were generated by transposase-mediated imprecise excisions of DNA by mobilizing two independent P-elements, P{EPgy2}Dab[EY10190] and P{XP}Dab[d11255], respectively (obtained from the Bloomington Stock Center and the Exelixis Collection at Harvard, respectively) and screening by PCR. Dab^1 and Dab^2 have deletion mutations and lack 5′ promoter and coding region of the *Dab* gene. We confirmed that both alleles are protein-null in the animal (Fig. 1). The hetero-allelic null mutant Dab^1/Dab^2 is viable and fertile. We used Dab^1/Dab^2 females for maternal zygote experiments.

Sources of fly stocks were as follows: Abl^2 and *sca-Gal4*, C. S. Goodman (PhyloTech, San Francisco, CA, USA); Abl^4, UAS-*Abl*, ena^{GC1}, ena^{GC5}, UAS-*Dab*, D. Van Vactor (Harvard University, MA, USA); *elav-Gal4*, Y. N. Jan (UCSF, CA, USA); *Df(3L)std11* and *Df(3L)st100.62*, E. Liebl (Dennison University, OH, USA). $trio^1$ and $trio^8$ were from the Bloomington *Drosophila* Stock Center. Balancer chromosomes containing β-galactosidase [β-gal (TM6B-T8-*lacZ* and CyO-*act-lacZ*)] and green fluorescent protein [GFP (TM3-*act*-GFP and CyO-*kruppel*-GFP)] expression markers were used in all genetic experiments.

Abl antibody generation

A fragment of *Drosophila* Abl kinase (including the kinase domain) was cloned into pQE 6X His vector (Qiagen). Expression was induced using 1 mM isopropyl β-D-1-thiogalactopyranoside (IPTG) in M15 competent cells. Induced Abl kinase protein was purified under denaturing conditions [8M urea, 25 mM Tris (pH 7.6), 100 mM NaCl, 0.5 mM phenylmethylsulfonyl fluoride (PMSF) and protease and phosphatase inhibitors (Sigma)] using Ni-NTA agarose beads (Qiagen) in Poly-Prep chromatography columns (Bio-Rad) to pull down the His-tagged Abl fragment. Purified Abl protein was dialyzed (Slide-A-Lyzer, Pierce) and refolded in refolding Buffer (0.1 M Tris, 0.4 M L-Arginine, 1 mM EDTA and Phosphatase and protease inhibitors) supplemented with decreasing amounts of urea. Purified Abl protein was injected into two New Zealand White rabbits (Covance Research) and sera obtained from different bleeds were tested for their specificity.

Immunohistochemistry and immunoblotting

Embryos to be used for immunostaining were collected, fixed and stained by standard methods as described previously (Bodmer et al., 1987). For phalloidin staining, fixed embryos were mechanically devitellinized by placing them under a coverglass and cracking them with gentle tapping. For axonal detection, anti-FasII (1D4, Hybridoma Bank, Iowa, USA) was used at 1:50. Biotinylated secondary antibody (Jackson ImmunoResearch Laboratories) staining was amplified using Vectastain Elite tertiary reagent (Vector Labs) and visualized using 3,3′-diaminobenzidine (DAB). Embryos were filleted in 90% glycerol in PBS. Embryos without the balancer chromosome were selected by anti-β-gal staining (1:1000; Cappel). Epithelial morphogenesis was analyzed using anti-Ena (1:100; 5G2, Hydridoma Bank, Iowa, USA), anti-phosphotyrosine (1:500; 4G10, Millipore), anti-β-tubulin (1:150; E7, Hybridoma Bank, Iowa, USA) and anti-Abl (1:300), fluorochrome-conjugated secondary antibodies (Jackson ImmunoResearch Laboratories) for the detection of primary antibodies, and rhodamine-phalloidin (Molecular Probes) and DAPI (Invitrogen) for the detection of F-actin and nuclei, respectively. For Dab protein detection, mouse monoclonal antibodies (P4D11, 1:2 and P6E11, Ascites 1:20 Hybridoma Bank, Iowa, USA) were used for immunoprecipitation-western experiments and a mouse polyclonal antibody (Le Gall et al., 2008) was used at 1:20 for immunohistochemistry. Anti-Ena (1:500), anti-Abl (1:1500) and anti-β-tubulin (1:750) were used for western blotting.

For eye disc immunostaining, late third-instar larval eye and antennal discs were dissected with the two brain lobes and fixed in 4% paraformaldehyde for 20 minutes at room temperature. The following antibodies were used: rabbit anti-Abl (1:300), rat anti-Elav 7E8A10 (1:20; Developmental Studies Hybridoma Bank) and rhodamine-phalloidin. *Z*-stacks were collected using a Zeiss LSM510 Confocal microscope at 63× magnification.

Quantification and statistical analysis.

For axonal analysis, hemisegments A2-A7 were used for analyzing intersegmental nerve b (ISNb) and segmental nerve a (SNa) defects. *P*-values were determined using the χ^2 test. For epithelial analysis, images of embryos at mid-cellularization were taken by confocal microscopy and imported to the NIH image software, Image J. For quantification of the apical region, an area encompassing the most apical 5% to the surface was measured. Equivalent apical areas (30 μm^2) were randomly selected for measurement. Lateral cortical accumulation was analyzed using profiles of fluorescence intensity from single planes. Ten cells from each of three embryos were examined per control and testing sample. Data were statistically analyzed using Student's *t*-test.

RESULTS

Generation of *Dab* mutation

Two unrelated P-elements, P{EPgy2}Dab[EY10190] and P{XP}Dab[d11255], derived from different collections, were used as starting points for imprecise excision experiments, and deletion mutations were isolated and identified from each. Screening of genomic DNA by PCR yielded two independent alleles, Dab^1 and Dab^2. The alleles have deletions of 3070 bp and 1887 bp, respectively, in each case including the 5′ promoter region and the first exon encoding the translation start (Fig. 1A). We examined Dab protein expression from head lysates of each homozygous mutant and from the hetero-allelic combination. They all failed to show a band corresponding to Dab protein (~280 kDa) on western blots (Fig. 1B). In addition, CNS axon accumulation of Dab was not detectable in *Dab* mutant embryos derived from *Dab* mutant mothers (here called Dab^{MZ} embryos) (Fig. 1C). Therefore, our molecular and biochemical evidence suggests that Dab^1 and Dab^2 are null alleles. Furthermore, Dab alleles complement mutations in the next upstream locus, *Lasp*, indicating that this gene is not affected. Homozygotes for both *Dab* alleles are viable and hetero-allelic Dab^1/Dab^2 flies are viable and fertile, allowing us to establish Dab^{MZ}, a stock that allows recovery of embryos that lack all maternal and zygotic Dab (65-90% adult viability, depending on the alleles used).

Dab is required for proper growth and guidance of motor axons

Dab mutant embryos display abnormal patterning of motor axons. In the wild type, the eight axons of intersegmental nerve b (ISNb) innervate a field of ventrolateral body wall muscles (Fig. 2A,B). In

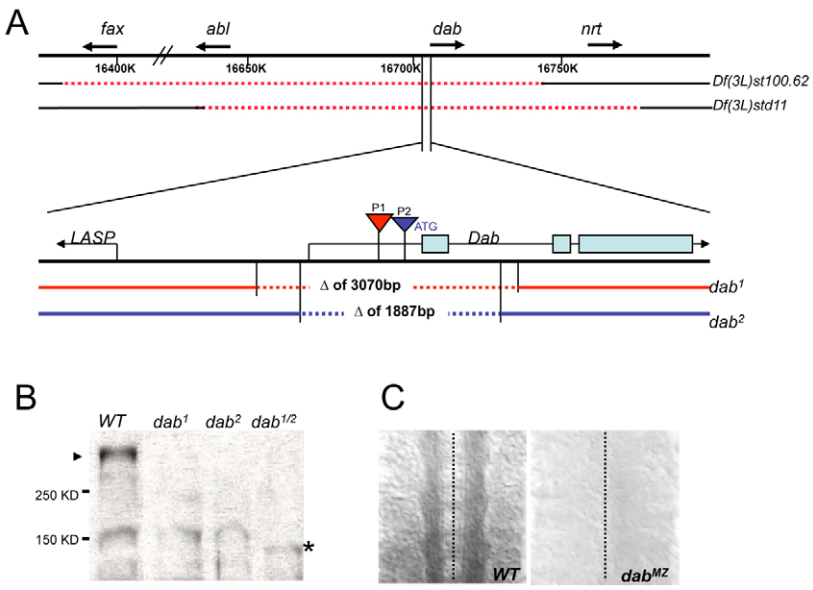

Fig. 1. Generation of Dab mutations. (**A**) Schematic representation of the Dab genomic region, indicating deficiencies, *Dab* mutations and selected genes. Two independent deficiencies, *Df(3L)st100.62* and *Df(3L)std11* were used for genetic interaction experiments. *Df(3L)st100.62* deletes genes including *fax, Abl* and *Dab*. *Df(3L)std11* deletes genes including *Abl, Dab* and *Nrt*. Two independent P-elements, P{EPgy2}Dab[EY10190] (P1) and P{XP}Dab[d11255] (P2), were mobilized out of the chromosome to yield imprecise excisions. Two deletion mutations (Dab^1 and Dab^2) derived from the two P-elements were isolated and lack 3070 bp and 1887 bp, respectively including the 5′ promoter region and first exon (representing codons 1-36). Size of deletions was confirmed by DNA sequencing (not shown). (**B**) Anti-Dab Western blot of Dab immunoprecipitated from adult head lysate. Dab protein (wild-type size 280 kDa; arrowhead) was not detectable in either homozygote mutants nor in a hetero-allelic combination. The lower band at ~150 kDa is a non-specific band (asterisk). The western blot was probed with mAb P6E11, which recognizes an epitope that is common to both Dab isoforms (Gertler et al., 1993) and that is well beyond the region deleted by the mutations. Similar results were obtained in a western blot using a polyclonal antibody raised against the N-terminal two-thirds of the protein (data not shown). (**C**) Anti-Dab immunohistochemistry in late stage 16 embryos using the polyclonal serum. Dab is expressed in axons of the CNS; however, the signal is absent in Dab^{MZ}, an embryo that lacks both maternal and zygotic Dab.

the *Dab* mutants, these axons stalled and failed to innervate their most distal target muscle, muscle 12 (defects are seen in 46% of total hemisegments in Dab^{MZ}/Dab^1 versus 2% in *Dab* heterozygote embryos; Fig. 2C and Table 1). In addition, we found analogous defects in another motor nerve, segmental nerve a (SNa). Normally, SNa diverges into dorsal and lateral branches with dorsal branch axons innervating muscles 21, 22 ,23 and 24 (Fig. 3A,B). However, Dab^{MZ} dorsal branch SNa axons often stopped short and failed to reach their muscle target (39% of hemisegments affected; Fig. 3C and Table 1). The same defects were observed in the zygotic *Dab* mutant but at much lower expressivity (9% in homozygous Dab^1; Table 1), suggesting a large maternal contribution to Dab function. The motor axon defects in maternal-zygote Dab-null mutants were largely rescued by expression of a *Dab* transgene with pan-neuronal drivers (41% rescue with *elav-Gal4* and 62% rescue with *scabrous-Gal4*; Fig. 2F, Fig. 3F and Table 1), further confirming the specificity of the mutant phenotype and demonstrating that Dab function is, at least partially, autonomous within the nervous system.

Genetic interactions with *Abl*, *ena* and *trio*

The axonal phenotypes of *Dab* mutants were quite similar to those of mutants in the Abl signaling pathway. For example, the ISNb phenotype of *Dab* mutants was similar to that of the *Abl* and *trio* mutants (Fig. 2D,E) described previously (Awasaki et al., 2000; Wills et al., 1999b). Moreover, SNa axons stall in both *Abl* and *trio* mutants, and we find that in both cases the mutations selectively disrupt the dorsal branch of SNa, as did mutation of *Dab* (Fig. 3D,E).

We next asked whether *Dab* interacts genetically with Abl signaling components by using deficiency chromosomes to reduce the dosage of *Abl* and its interacting partners in the *Dab* mutant background. Dab^{MZ} axon phenotypes were dramatically enhanced in the presence of deficiency chromosomes (Table 1). The moderate expressivity of ISNb axon defects in Dab^{MZ} (46%) was increased by heterozygosity for deficiency chromosomes reducing gene copies of *Abl* and *Nrt* [77% with *Df(3L)std11/+*], or *Abl* and *fax* [65% with *Df(3L)st100.62/+*]. These interactions were observed for both Dab^1 and Dab^2. An analogous synergistic interaction was observed for SNa (Table 1). We found that *Abl* is the major gene in the deficiencies that contributes to this interaction, because a single copy of a wild-type *Abl* genomic transgene rescued the synergistic interaction, as assessed in ISNb using *Df(3L)std11*, back to the level of the *Dab* mutant alone (from 77% defective to 42%). We also examined interactions of two other mutants in the Abl pathway, *trio* and *ena,* in the *Dab* null environment. *trio* mutations similarly enhanced *Dab* ISNb axon defects (78% with $trio^1/+$ and 80% with $trio^8/+$, Table 1). Conversely, heterozygous loss-of-function mutations of the *Abl* antagonist *ena* suppressed the Dab phenotype in ISNb axons (from 46% to 26% with $ena^{GC5}/+$, and to 36% with $ena^{GC1}/+$; Table 1).

Dab is genetically upstream of *Abl* and *ena*

As Dab^{MZ}-null embryos have a well-formed nervous system, we were able to perform classical genetic epistasis to determine the order of the pathway. We found that pan-neuronal overexpression of Abl suppressed the Dab^{MZ} ISNb phenotypes (46% to 29%; Table 1), whereas overexpression of Dab failed to suppress the

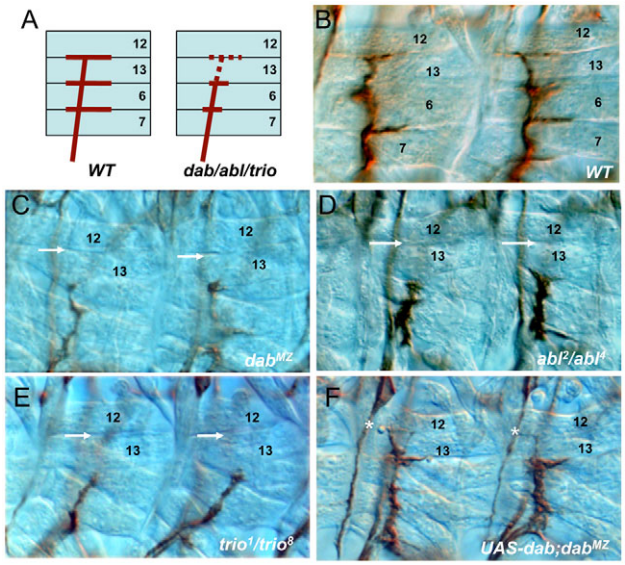

Fig. 2. Axonal phenotypes of intersegmental nerve b (ISNb) motor nerves. Embryos from early stage 17 were stained with anti-fasciclin II (1D4) and dissected. (**A**) Wild-type (WT) ISNb always displays three major synaptic innervations to ventral longitudinal muscles (VLM), whereas mutations in *Dab, Abl* and *trio* often display a common axonal defect: a failure of distal targeting to the muscle 12/13 cleft (red dotted line). (**B-E**) When compared with wild type (B), the same axonal defect is shown by Dab^{MZ} (C), Abl^{2}/Abl^{4} (D) and $trio^{1}/trio^{8}$ (E): a missing axon projection for distal muscle innervation (white arrows). (**F**) Neuronal rescue experiment. UAS-*Dab* transgene expression in Dab^{MZ} background, driven by an *elav-Gal4* driver, results in a notable rescue of the ISNb defect of Dab^{MZ} (white asterisks).

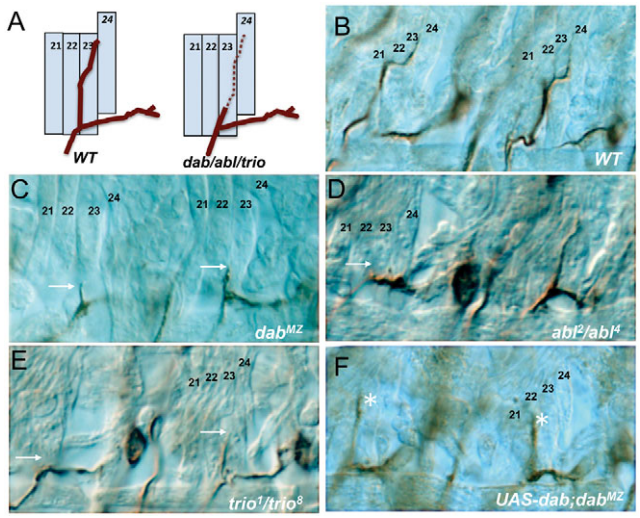

Fig. 3. Axonal phenotypes of segmental nerve a (SNa) motor nerves. (**A**) In the wild type, two major branches of the SNa are equally projected dorsally and laterally. Dorsally projected axons are normally targeted to muscles 21-24. However, *Dab, Abl* and *trio* mutants failed to show intact SNa dorsal targeting (red dotted line). (**B-E**) In Dab^{MZ} (C), Abl^{2}/Abl^{4} (D) *and* $trio^{1}/trio^{8}$ (E) mutants, dorsal axons commonly stop short (white arrows) in comparison with wild type (B), whereas lateral projections are mostly normal (placed in different focal plane in some pictures). (**F**) Neuronal expression of the Dab transgene. *elav-Gal4*-driven UAS-*Dab* in Dab^{MZ} partially restores dorsal projections (white asterisks).

highly penetrant ISNb phenotype of *Abl*. Together, these data suggest that *Abl* acts downstream of *Dab* (Table 1). Overexpression of Dab with the same Gal4 driver does significantly modify a different phenotype of these same ISNb axons; the bypass phenotype of a $Notch^{ts}$ mutant (Le Gall et al., 2008). This demonstrates that the level of Dab overexpression achieved in this experiment was sufficient to significantly modulate the growth of ISNb axons, and thus validates our interpretation of the *Abl*/*Dab* epistasis experiment. As it has been demonstrated previously that Ena acts downstream of Abl (Gates et al., 2007; Grevengoed et al., 2003), we next examined the genetic epistasis between *Dab* and *ena*. The severe axonal defects of *ena* mutants (99% ISNb bypass of ena^{GC1}/ena^{GC5}) were not suppressed by reduction of Dab function (Table1), whereas *ena* mutations significantly suppress *Dab* axon phenotypes as described above. These results suggest that *Dab* acts genetically upstream of *ena*, as well as *Abl*.

Dab functions in Abl-dependent epithelial morphogenesis

In addition to its roles in axon patterning, Abl is required for several aspects of epithelial morphogenesis in the early embryo. Maternal-zygote *Abl* mutants display defects during syncytial pseudocleavage and cellularization (Grevengoed et al., 2003), ventral furrow formation (Fox and Peifer, 2007), and dorsal closure (Grevengoed et al., 2001). We therefore examined epithelial morphogenesis in Dab^{MZ} embryos.

We first investigated the syncytial pseudocleavage and cellularization of Dab^{MZ} embryos and found that they mimicked *Abl* phenotypes (Grevengoed et al., 2003) in this context. As observed for *Abl* mutants, absence of Dab caused abnormal compartmentalization, such as anucleated pseudocells (Fig. 4A, short white arrows), incomplete pseudocleavage furrows and multi-nucleated cells (Fig. 4A, long yellow arrows) during cellularization (92% of embryos display defective cells; n=51). However, the microtubule baskets surrounding each nucleus in multinucleated cells looked normal (Fig. 4A). Previously, it has been shown that F-actin in *Abl* maternal-zygote mutants was apically accumulated (Grevengoed et al., 2003). Similarly, Dab^{MZ} mutants exhibited abnormal apical actin accumulation throughout cellularization (Fig. 4B). At mid-cellularization, for example, overall apical F-actin in Dab^{MZ} mutants was increased by ~49% (Fig. 4C).

Ena and Abl localization are disrupted in Dab^{MZ} mutant

In addition to the apical accumulation of actin in cellularizing Dab^{MZ} mutant embryos, we observed correlated alterations of actin, phosphotyrosine and Enabled protein localization at a mid-lateral level in this epithelium. The mid-lateral localization of actin was extremely variegated, with patches of contiguous pseudocells showing a disrupted actin pattern. Wild-type embryos, by contrast, displayed uniform lateral actin localization (Fig. 5A). The fluctuations in actin localization were strongly correlated with fluctuations in phosphotyrosine accumulation (Fig. 5B). The subcellular distribution of Enabled protein was also highly variegated at a mid-lateral level in Dab^{MZ}, but in a pattern that was complementary to that of actin and phosphotyrosine. Thus, in places along the mid-lateral cortex of the pseudocells where F-actin was reduced, Ena was selectively enriched (Fig. 6B). In such

Table 1. Quantification of axonal defects in *Dab* mutants and genetic interactions

Genotype	Modifier	Hemisegments exhibiting indicated defect (%)	*n*	Control (percentage exhibiting defect)	
ISNb stall					
Dab^{MZ}/ Dab^{1}	+/+	46	726	Dab^{MZ}/+	(9)‡
	UAS-Dab (elav-Gal4)	27	144	*UAS-Dab (elav-Gal4)*	(<1)
	Df(3L)std11/+	77	390	*Df Std11/+*	(11)‡
	*Df(3L)std11,P[Abl]/+**	42	143	*P[Abl]/+*	(<1)
	Df(3L)st100.62/+	65	192	*Df(3L)st100.62/+*	(8)‡
	$trio^{1}$/+	78	288	$trio^{1}$/+	(3)‡
	$trio^{8}$/+	80	256	$trio^{8}$/+	(2)
	ena^{GC5}/+	26	252	ena^{GC5}/+	(<1)
	ena^{GC1}/+	36	228	ena^{GC1}/+	(<1)
	UAS-Abl (elav-Gal4)†	29	120	*UAS-Abl (elav-Gal4)*	(<1)
Dab^{MZ}/ Dab^{2}	+/+	59	570	Dab^{MZ}/+	(9)‡
	Df(3L)std11/+	78	180	*Df(3L)std11/+*	(11)‡
	UAS-Dab (sca-Gal4)	22	228	*UAS-Dab (sca-Gal4)*	(<1)
Dab^{1}/ Dab^{1}	+/+	9	1136		
	Df(3L)std11/+	59	240	*Df(3L)std11/+*	(11)‡
	Df(3L)st100.62/+	54	276	*Df(3L)st100.62/+*	(8)‡
	$trio^{1}$/+	72	168	$trio^{1}$/+	(3)‡
Abl^{2}/ Abl^{4}	+/+	77	120		
	UAS-Dab (elav-Gal4)	82	132	*UAS-Dab (elav-Gal4)*	(<1)
ISNb bypass					
ena^{GC1}/ ena^{GC5}	+/+	99	180		
	Dab^{1}/+	99	240	Dab^{1}/+	(<1)
SNa stop short					
Dab^{MZ}/ Dab^{1}	+/+	39	150	Dab^{MZ}/+	(5)
	Df(3L)std11/+	69	238	*Df(3L)std11/+*	(9)‡
	*Df(3L)std11/+,P[Abl]/+**	39	132	*P[Abl]/+*	(<1)
	Df(3L)st100.62/+	57	168	*Df(3L)st100.62/+*	(8)
	$trio^{1}$/+	80	168	$trio^{1}$/+	(1)
Dab^{MZ}/ Dab^{2}	+/+	33	132		
	Df(3L)std11/+	62	180	*Df(3L)std11/+*	(9)‡
Dab^{1}/ Dab^{1}	+/+	9	1136		
	Df(3L)std11/+	52	204	*Df(3L)std11/+*	(9)‡
	$trio^{1}$/+	35	240	$trio^{1}$/+	(2)

Early stage 17 embryos were fixed, stained with anti-FasII (1D4) and dissected. Hemisegments A2-A7 were analyzed for the scoring of ISNb (stall or bypass) and SNa defects (stop short of dorsal branch in Fig. 3). 'ISNb bypass' is a completely different defect from 'ISNb stall'. ISNb axons do not enter the ventral longitudinal muscles, rather they bypass along the ISN root. *P*-values were determined by χ^2 test. All comparisons are statistically significant ($P<0.001$). Unless otherwise indicated, the comparison is between the homozygote mutant with and without the indicated modifier.

*In the case of Dab^{MZ}/*Df(3L)std11,P[Abl]*, the comparison is with Dab^{MZ}/*Df(3L)std11* stall.

†In addition to the stall phenotype, 25% of total hemisegments display bypass phenotypes. In the Dab^{MZ}/ Dab^{1} background, the expressivity of ISNb bypass is increased to 33%.

‡In some cases, the same control genotype is the appropriate comparison for more than one experimental genotype. In these cases, data for the control genotype were pooled and that value is presented for all applicable table entries.

domains, cortical Ena was increased by 66-230% (Fig. 6D). Some cells with high levels of Enabled displayed a constricted morphology with the nucleus either displaced or completely absent (Fig. 6C, dotted rectangle). Western blot analysis did not reveal any difference in overall levels of Ena protein between wild-type and Dab^{MZ} cellular blastoderm stage embryos (Fig. 6E), suggesting that Dab regulates the subcellular localization of Ena rather than its expression level.

The hypothesis that Dab specifically controls Ena localization is further supported by analysis of Dab function during a different example of epithelial morphogenesis: dorsal closure. Like Abl^{MZ} mutants (Grevengoed et al., 2001), Dab^{MZ} mutants had disrupted dorsal closure with occasional breaks of the leading edge, failure of cell elongation (Fig. 7B,D) and disturbances in the 'zippering' of the dorsal epithelia (Fig. 7F). Visualization of Ena protein in the associated amnioserosa cells revealed that, here too, the subcellular localization of Ena was severely disturbed in Dab^{MZ} mutants (Fig. 7H,J). Taken together with the data on cellularization, the disrupted subcellular localization of Ena in Dab^{MZ} mutants implies that Ena is downstream of Dab in the genetic pathway.

We also examined the subcellular localization of Abl in Dab^{MZ} mutants. In the wild type, Abl was present homogenously across the embryo at the cellularization stage with only slight accumulation in mid-lateral membranes (Fig. 8A). In Dab^{MZ} mutants, Abl localization was substantially increased at cell junctions (Fig. 8B). At this apicobasal position, where correlated fluctuations were seen in actin and phosphotyrosine signals, the level of Abl protein was often seen to vary in parallel (Fig. 8B). However, there are also sites where increased Abl concentration is seen even though the actin signal remained normal (Fig. 8C). This suggests that Disabled may directly regulate the subcellular localization of Abl protein. This was confirmed by examining Abl localization in the retinal neuroepithelium in developing eye discs. In wild type animals, Abl was uniformly enriched along the membranes of developing photoreceptors (Fig. 9A). In Dab^{MZ}

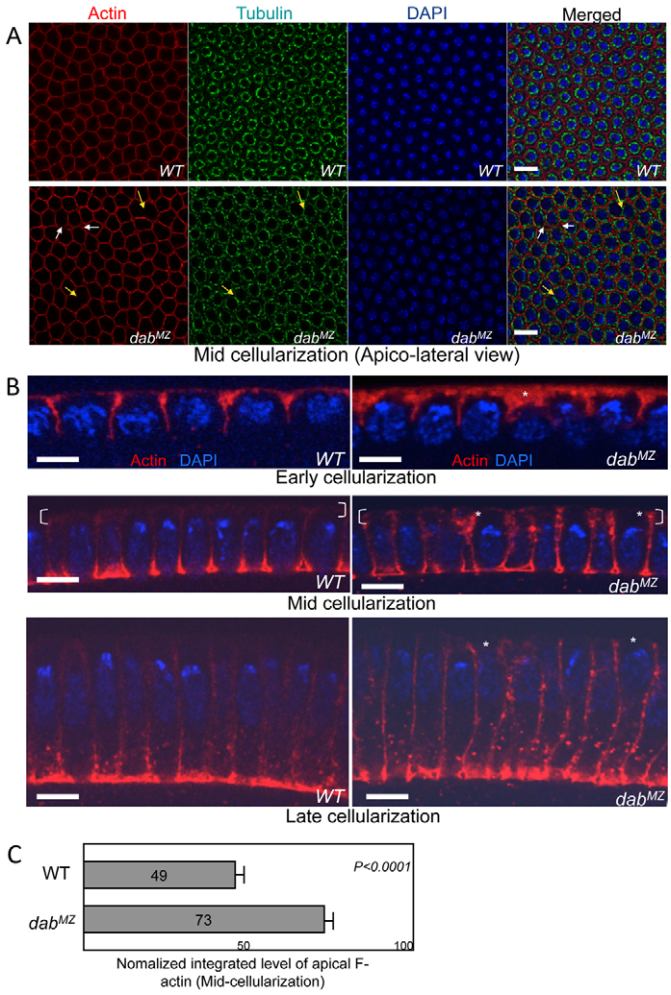

Fig. 4. Epithelial morphogenetic defects in *Dab^{MZ}* during cellularization. (**A**) Embryos at mid-cellularization were stained with phalloidin (to visualize F-actin; red), anti-tubulin (green) and DAPI (blue). In an apicolateral view, *Dab^{MZ}* embryos display partial or complete absence of cortical actin formation in a fraction of cells, resulting in multinucleate cells (yellow arrows in red channel) and also have small pseudocells with no nuclei (white arrows). However, the formation of peri-nuclear tubulin baskets appears to be normal (yellow arrows in green channel). Scale bar: 10 μm. (**B**) Cross-section views through cellularizing embryos. Phalloidin staining (F-actin) is in red and DAPI (DNA) in blue. Apicolateral F-actin accumulates irregularly and at elevated levels in *Dab^{MZ}* (white asterisks). Scale bar: 10 μm. (**C**) Quantification of apical actin accumulation at mid-cellularization. F-actin signal in the most apical 5% of the cells was quantified (white brackets in B, for example) by integrating the fluorescent signal. Raw data were normalized to a scale from zero to 100. Data presented are mean ± s.e.m. Apical actin is increased by 49% in *Dab^{MZ}* relative to wild type (WT; $P<0.0001$).

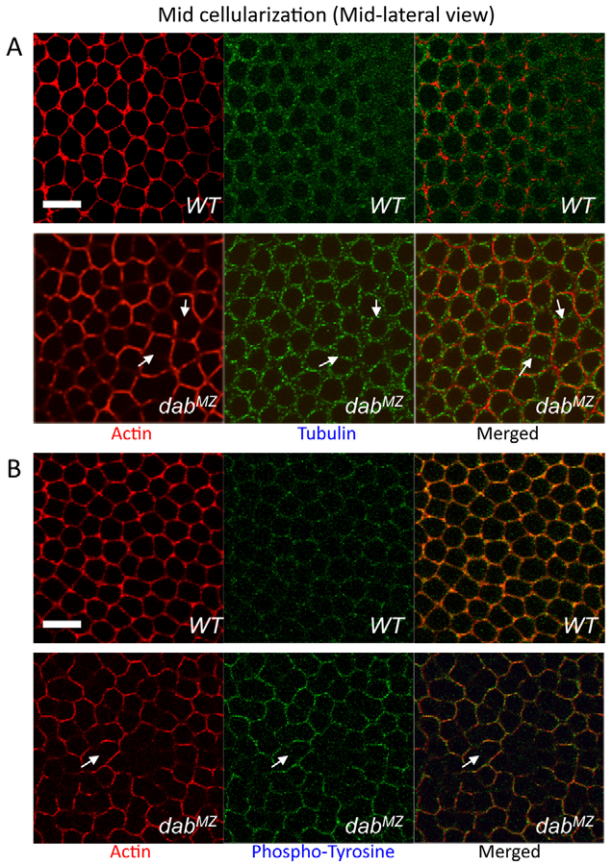

Fig. 5. Variable lateral actin accumulation in *Dab^{MZ}*. (**A**,**B**) Embryos at mid-cellularization were stained with a combination of phalloidin (F-actin) and either anti-tubulin (A) or anti-phosphotyrosine (B). At a mid-lateral level (more basal than that shown in Fig. 4A), the intensity of the actin signal is highly variable in *Dab^{MZ}*, with patches of greatly reduced actin accumulation (arrows in red channel). By contrast, the level of tubulin accumulation is homogeneous (green channel in A). The cortical phospho-tyrosine level fluctuates in register with actin fluctuations in *Dab^{MZ}* (arrows). Scale bars: 10 μm.

mutants, conversely, there is significant disruption of Abl localization, with the cortical accumulation disturbed or lost in large patches of photoreceptor clusters (Fig. 9B). Unlike the blastoderm, however, overall F-actin organization was largely unaffected by *Dab* in the eye disc, with only scattered, relatively minor effects on actin structure (Fig. 9D). This supports the hypothesis that altered subcellular localization of Abl in the *Dab* mutant eye disc is a direct consequence of the absence of *Dab* function and not secondary to generalized disruption of actin patterning. Thus, altered Abl distribution in the absence of Dab suggests that Abl protein localization is downstream of Dab, consistent with the genetic data presented above. Together, these data strongly support the hypothesis that Dab acts upstream of Abl and Ena.

DISCUSSION

Data presented here demonstrate that Disabled is a bona fide component of the Abl signaling pathway. *Dab^{MZ}* embryos showed *Abl*-like phenotypes in different contexts: axon patterning, dorsal closure and cellularization. *Dab* interacts genetically with *Abl* and its genetic co-factors *trio* and *ena* during motor axon guidance, and is a positive regulator of Abl pathway signaling, acting upstream of Abl and Ena. Although the *Dab* mutant phenotypes mimicked *Abl* phenotypes, they were consistently milder. For example, the expressivity of the ISNb and SNa phenotypes of *Dab^{MZ}* was rather less than those of *Abl*. Similarly, the extent of Ena and actin accumulation in the apical region of blastoderm cells of *Dab^{MZ}* (up to 82% increase; data not shown) was rather less than the three- to fivefold increase reported previously for *Abl^{MZ}* mutants

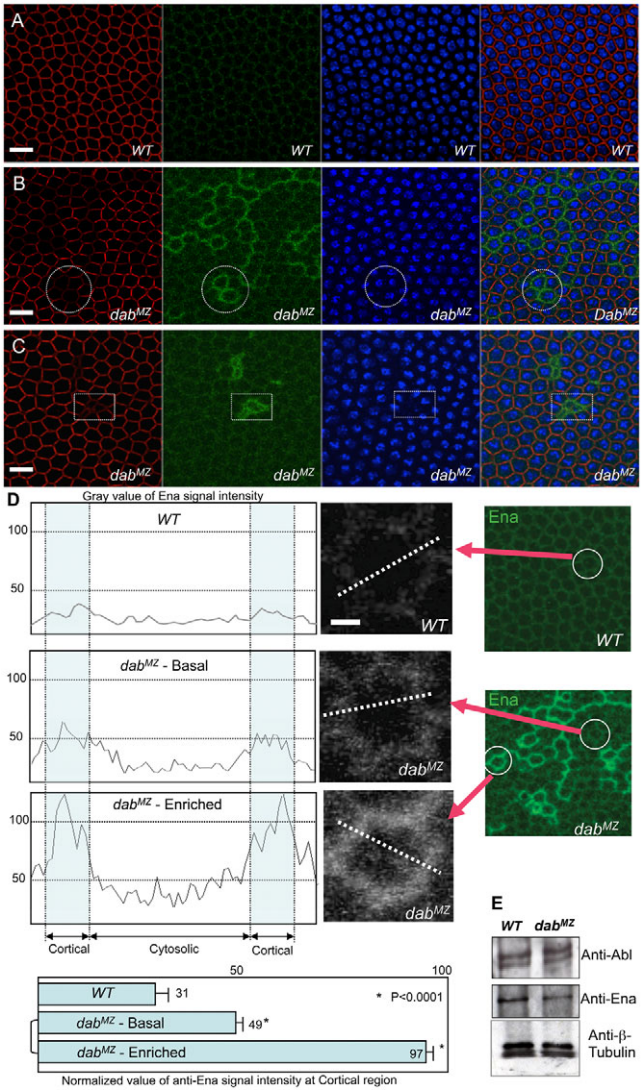

Fig. 6. Subcellular localization of Ena is altered in *Dab^{MZ}*. (**A-C**) Embryos were labeled with phalloidin (F-actin; red), anti-Ena (green) and DAPI (blue). Mid-lateral views of mid-cellularization in wild type (A) and *Dab^{MZ}* (B,C). (A) Ena is slightly enriched at the cell periphery in the wild type. (B) Ena is highly accumulated at the cortical regions of some cells in *Dab^{MZ}*, corresponding to those places where the actin level is significantly reduced (white dotted circles, for example). (C) Ena accumulates at very high levels in pseudocells missing their nuclei, which also have reduced actin level at this focal plane (white dotted rectangles). Scale bars: 10 μm. (**D**) Quantification of cortical Ena localization. Confocal images were imported to Image J software and a line profile of fluorescence intensity was determined in the position of the dotted line (examples shown). Scale bar: 1 μm. Raw values of integrated Ena signal intensity in wild type and *Dab^{MZ}* were normalized to a scale from zero to 100. Ten cells in three embryos of each type (wild type, basal in *Dab^{MZ}* and enriched in *Dab^{MZ}*) were measured. * Statistical significance was determined by Student's *t*-test ($P<0.0001$). Data presented in histogram are mean ± s.e.m. (**E**) Immunoblots of lysates from wild-type (WT) and *Dab^{MZ}* cellularizing embryos. β-tubulin was used as a loading control.

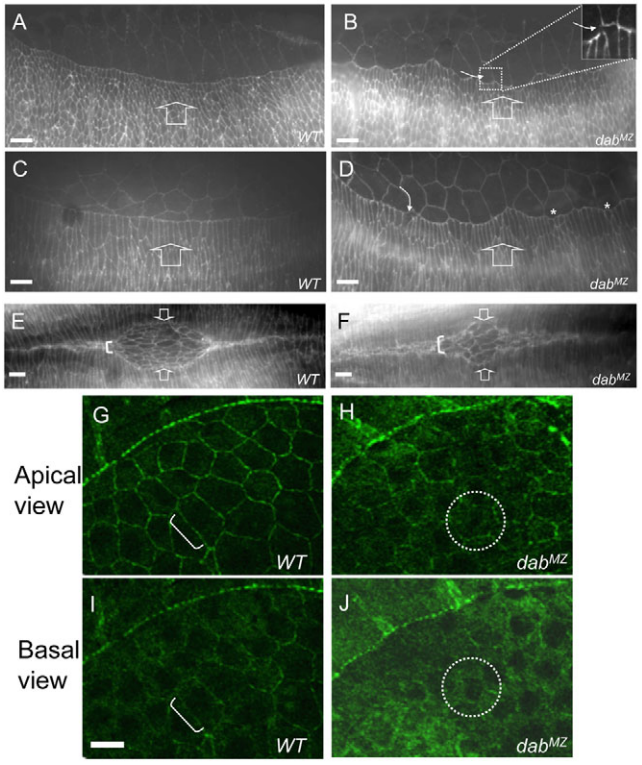

Fig. 7. Epithelial morphogenetic defects in *Dab^{MZ}* during dorsal closure. (A-F) Embryos were stained with anti-phosphotyrosine. (**A**,**B**) In the wild type (A) at stage 13, the leading edge of dorsally extending epithelial cells produces a smooth, continuous line, whereas in *Dab^{MZ}* (B) the leading edge is jagged and irregular with occasional discontinuities (white curved arrow in inset). (**C**,**D**) At stage 14, wild-type (C) leading cells elongate dramatically. Leading cells of *Dab^{MZ}* (D) also elongate, but irregularly (curved arrow), with some cells failing to elongate (asterisks). (**E**,**F**) In wild type (E), apposed leading edges 'zip' together smoothly from the embryo termini towards the eye-shaped central region. In *Dab^{MZ}*, the final 'zippering' of the leading edges is not as tight as in the wild type, leading to abnormal shape of amnioserosa and loose association of the apposed epithelia (white bracket). Broad arrows indicate the direction of epithelial migration (A-F). (**G-J**) Ena subcellular localization in amnioserosa cells. Embryos were stained with anti-Ena at stage 14. (G) At the apical level in the wild type (G), Ena is tightly localized to the cortical membrane (white bracket) but in the *Dab^{MZ}* mutant (H), Ena is greatly decreased and loosely localized to the membrane with some cytosolic distribution (white dotted circle, for example). The basal view (I,J) shows Ena mostly localized to the cortical region (white bracket) in the wild type (I) but an overall increase in basal Ena that is homogenously distributed across the cell in the mutant (J; white dotted circle). Scale bar: 10 μm.

(Grevengoed et al., 2003). This suggests that although Dab contributes significantly to Abl pathway activity, it is not absolutely essential.

Dominant genetic interactions have been used to identify components of the Abl pathway (Hill et al., 1995), but it has not been possible to determine their order. Here, because we could examine the true null phenotypes of *Dab*, we have been able to perform classical epistasis and find that *Dab* acts genetically upstream of *Abl* and *ena*: altering Abl or Ena levels modified the *Dab* phenotype, but changing Dab could not alter an *Abl* or *ena* phenotype. This was confirmed by functional experiments as Abl and Ena localization required Dab during the cellularization of the blastoderm. Strikingly, Abl and Ena did not simply colocalize with the altered actin distribution in *Dab^{MZ}*; Abl was disrupted even in places where actin was not, and Ena disruptions were largely

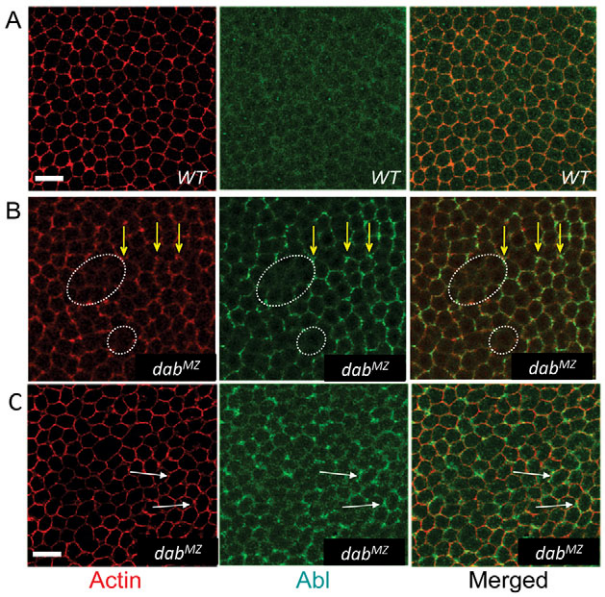

Fig. 8. Subcellular localization of Abl is altered in *Dab*^{MZ} embryos. (**A-C**) Mid-lateral view of mid-cellularization. Embryos were stained with phalloidin (F-actin) and anti-Abl. In the *Dab*^{MZ} mutant (B,C), cortical localization of actin is variable or absent in places at this focal plane. Abl is substantially, but irregularly, increased, particularly at junctions of cells with relatively increased levels of F-actin (yellow arrows). Where Abl level is low (roughly equivalent to the Abl level in wild type), F-actin staining is often reduced or absent (white dotted circles). However, Abl is also found to be highly accumulated at sites with apparently wild-type levels of actin (white arrows in C). Scale bar: 10 μm.

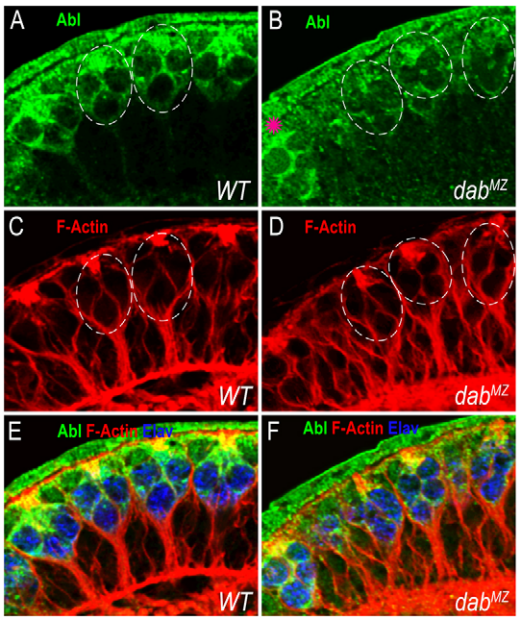

Fig. 9. Disabled is required for Abl localization in the retinal neuroepithelium. (**A-F**) Cross-section of a third instar larval eye disc, stained with anti-Abl (green), phalloidin (F-actin; red) and anti-Elav (to identify photoreceptors; blue). Posterior is to the left; morphogenetic furrow is 12-18 rows of photoreceptor clusters to the right. In the wild type, Abl protein (A) is enriched cortically along photoreceptor membranes and in an actin-rich apical tuft (dashed ovals). In *Dab*^{MZ} mutants, cortical Abl accumulation (B) is strongly disrupted in patches of photoreceptor clusters (dashed ovals), though it is still observed in adjacent clusters (pink star). (C) In the wild type, F-actin is uniformly distributed along the photoreceptor membrane and axons and is strongly expressed at the apical region of the cell. (D) In *Dab*^{MZ} mutants, F-actin distribution is largely normal, including in clusters with disrupted Abl localization (dashed ovals). (E,F) Overlay of (A,C) and (B,D), respectively. Photoreceptor nuclei are labeled with anti-Elav.

complementary to those of actin. Moreover, Abl localization was disrupted in developing larval eye discs in *Dab* mutants, even though actin structure was largely normal. This suggests that the effect of Dab on Abl and Ena localization is specific, not just secondary to disruption of F-actin.

Analysis of the *Dab* phenotypes in epithelial morphogenesis was particularly informative for illuminating the role of this protein in actin organization and its physical relationship to other components of the Abl pathway. In syncytial-stage *Dab*-null embryos, for example, in the mid-lateral region of the developing epithelium, we found that sites with high accumulation of Abl protein also had high phosphotyrosine content and a distribution of F-actin either equivalent to that in wild type or slightly elevated. By contrast, nearby regions without elevated Abl generally had reduced phosphotyrosine and lacked distinct F-actin staining, and these domains had elevated and delocalized Enabled. These data are consistent with the hypothesis of Peifer and co-workers (Gates et al., 2007; Stevens et al., 2008) that a key role of Abl is to exclude Enabled, thereby controlling actin distribution. Our data further suggest that Dab controls actin structure in this portion of the epithelium, in part, by controlling the distribution and activity of Abl, and therefore of Ena. One plausible hypothesis is that formation of proper actin structure requires a threshold level of Abl activity, and that, in the absence of Dab, high concentrations of Abl are required to achieve this threshold, whereas with the assistance of Dab, low homogeneous levels of Abl suffice. It is also noteworthy that the correlations we observe in localization of the various proteins at the blastoderm stage were selective for the mid-lateral level of the epithelium. Evidently, different molecular mechanisms are limiting for actin organization at different positions along the apicobasal axis.

The modest *Abl*-like phenotype of *Dab*^{MZ} in blastoderm stage cells manifests as a stochastic mixture of states: one close to (but distinguishable from) wild type and the other clearly aberrant. The switch between the two states is not strictly cell autonomous but heavily influenced by intercellular communication in this syncytial epithelium. Thus, strongly affected cells are almost never found in isolation but rather as strings or domains of contacting cells and cell membranes. Indeed, different cell-cell interfaces of a single cell can have clearly different patterns of Ena accumulation. Evidently, cell-cell contacts strongly influence the local structure of the cytoskeleton in these cells. The observation that intercellular communication coordinates cytoskeletal structure in the morphogenesis of this epithelium is reminiscent of observations of other epithelia, including planar cell polarity (Chen et al., 2008), coordination of ventral furrow involution (Parks and Wieschaus, 1991) and the function of the actin purse-string in dorsal closure (Kiehart et al., 2000). It is possible that such intercellular coordination of cell morphogenesis is a common feature of epithelial development.

In mammals, Dab is required for reelin-dependent localization of cortical neurons. This is mediated by interaction with Notch (Hashimoto-Torii et al., 2008; Sibbe et al., 2009). Our previous studies first identified a crucial Notch-Dab interaction in the context of embryonic axon patterning in the fly, based on studies

from biochemistry and gain-of-function experiments (Le Gall et al., 2008), and we have now verified this with loss of function mutations (J.K.S. and E.G., unpublished). The finding that Dab is a core element of Abl signaling raises the issue of whether Abl may also be involved in the Dab-dependent migration of mammalian cortical neurons, acting in parallel or together with Notch to control their position in response to reelin.

Acknowledgements
We thank Drs. M. Peifer, F. Gertler and C.-H. Lee for critical comments and members of our laboratories for helpful discussions; the Bloomington *Drosophila* Stock Center and Exelixis Collection at Harvard for Dab P-element insertion lines, and the Developmental Studies Hybridoma Bank for antibody reagents. This work was supported in part by the Intramural Research Program of NIH (NINDS: Z01NS003013 to E.G.). G.M. was supported by the Alzheimer Forschung Initiative eV and DFG., J.K.S. and M.M. were supported by NIH grant (EY014597). Deposited in PMC for release after 12 months.

Competing interests statement
The authors declare no competing financial interests.

References
Awasaki, T., Saito, M., Sone, M., Suzuki, E., Sakai, R., Ito, K. and Hama, C. (2000). The Drosophila trio plays an essential role in patterning of axons by regulating their directional extension. *Neuron* **26**, 119-131.
Barzik, M., Kotova, T. I., Higgs, H. N., Hazelwood, L., Hanein, D., Gertler, F. B. and Schafer, D. A. (2005). Ena/VASP proteins enhance actin polymerization in the presence of barbed end capping proteins. *J. Biol. Chem.* **280**, 28653-28662.
Bashaw, G. J., Kidd, T., Murray, D., Pawson, T. and Goodman, C. S. (2000). Repulsive axon guidance: Abelson and Enabled play opposing roles downstream of the roundabout receptor. *Cell* **101**, 703-715.
Bateman, J., Shu, H. and Van Vactor, D. (2000). The guanine nucleotide exchange factor trio mediates axonal development in the Drosophila embryo. *Neuron* **26**, 93-106.
Bodmer, R., Barbel, S., Sheperd, S., Jack, J. W., Jan, L. Y. and Jan, Y. N. (1987). Transformation of sensory organs by mutations of the cut locus of *D. melanogaster*. *Cell* **51**, 293-307.
Bear, J. E., Svitkina, T. M., Krause, M., Schafer, D. A., Loureiro, J. J., Strasser, G. A., Maly, I. V., Chaga, O. Y., Cooper, J. A., Borisy, G. G. et al. (2002). Antagonism between Ena/VASP proteins and actin filament capping regulates fibroblast motility. *Cell* **109**, 509-521.
Briancon-Marjollet, A., Ghogha, A., Nawabi, H., Triki, I., Auziol, C., Fromont, S., Piche, C., Enslen, H., Chebli, K., Cloutier, J. F. et al. (2008). Trio mediates netrin-1-induced Rac1 activation in axon outgrowth and guidance. *Mol. Cell. Biol.* **28**, 2314-2323.
Chen, W. S., Antic, D., Matis, M., Logan, C. Y., Povelones, M., Anderson, G. A., Nusse, R. and Axelrod, J. D. (2008). Asymmetric homotypic interactions of the atypical cadherin flamingo mediate intercellular polarity signaling. Cell **133**, 1093-1105.
Crowner, D., Le Gall, M., Gates, M. A. and Giniger, E. (2003). Notch steers Drosophila ISNb motor axons by regulating the Abl signaling pathway. *Curr. Biol.* **13**, 967-972.
Debant, A., Serra-Pages, C., Seipel, K., O'Brien, S., Tang, M., Park, S. H. and Streuli, M. (1996). The multidomain protein Trio binds the LAR transmembrane tyrosine phosphatase, contains a protein kinase domain, and has separate rac-specific and rho-specific guanine nucleotide exchange factor domains. *Proc. Natl. Acad. Sci. USA* **93**, 5466-5471.
Forsthoefel, D. J., Liebl, E. C., Kolodziej, P. A. and Seeger, M. A. (2005). The Abelson tyrosine kinase, the Trio GEF and Enabled interact with the Netrin receptor Frazzled in Drosophila. *Development* **132**, 1983-1994.
Fox, D. T. and Peifer, M. (2007). Abelson kinase (Abl) and RhoGEF2 regulate actin organization during cell constriction in Drosophila. *Development* **134**, 567-578.
Fremion, F., Darboux, I., Diano, M., Hipeau-Jacquotte, R., Seeger, M. A. and Piovant, M. (2000). Amalgam is a ligand for the transmembrane receptor neurotactin and is required for neurotactin-mediated cell adhesion and axon fasciculation in Drosophila. *EMBO J.* **19**, 4463-4472.
Gates, J., Mahaffey, J. P., Rogers, S. L., Emerson, M., Rogers, E. M., Sottile, S. L., Van Vactor, D., Gertler, F. B. and Peifer, M. (2007). Enabled plays key roles in embryonic epithelial morphogenesis in Drosophila. *Development* **134**, 2027-2039.
Gertler, F. B., Doctor, J. S. and Hoffmann, F. M. (1990). Genetic suppression of mutations in the Drosophila abl proto-oncogene homolog. *Science* **248**, 857-860.
Gertler, F. B., Hill, K. K., Clark, M. J. and Hoffmann, F. M. (1993). Dosage-sensitive modifiers of Drosophila abl tyrosine kinase function: prospero, a regulator of axonal outgrowth, and disabled, a novel tyrosine kinase substrate. *Genes Dev.* **7**, 441-453.
Gertler, F. B., Comer, A. R., Juang, J. L., Ahern, S. M., Clark, M J., Liebl, E. C. and Hoffmann, F. M. (1995). *enabled*, a dosage-sensitive suppressor of mutations in the *Drosophila* Abl tyrosine kinase, encodes an Abl substrate with SH3 domain-binding properties. *Genes Dev.* **9**, 521-533.
Gitai, Z., Yu, T., Lundquist, E., Tessier-Lavigne, M. and Bargmann, C. (2003). The netrin receptor UNC-40/DCC stimulates axon attraction and outgrowth through enabled and, in parallel, Rac and UNC-115/AbLIM. *Neuron* **37**, 53-65.
Grevengoed, E. E., Loureiro, J. J., Jesse, T. L. and Peifer, M. (2001). Abelson kinase regulates epithelial morphogenesis in Drosophila. *J. Cell Biol.* **155**, 1185-1198.
Grevengoed, E. E., Fox, D. T., Gates, J. and Peifer, M. (2003). Balancing different types of actin polymerization at distinct sites: roles for Abelson kinase and Enabled. *J. Cell Biol.* **163**, 1267-1279.
Hashimoto-Torii, K., Torii, M., Sarkisian, M. R., Bartley, C. M., Shen, J., Radtke, F., Gridley, T., Sestan, N. and Rakic, P. (2008). Interaction between Reelin and Notch signaling regulates neuronal migration in the cerebral cortex. Neuron **60**, 273-284.
Hill, K. K., Bedian, V., Juang, J. L. and Hoffmann, F. M. (1995). Genetic interactions between the Drosophila Abelson (Abl) tyrosine kinase and failed axon connections (fax), a novel protein in axon bundles. *Genetics* **141**, 595-606.
Hoffmann, F. M. (1991). Drosophila abl and genetic redundancy in signal transduction. *Trends Genet.* **7**, 351-355.
Howell, B. W., Gertler, F. B. and Cooper, J. A. (1997a). Mouse disabled (mDab1): a Src binding protein implicated in neuronal development. *EMBO J.* **16**, 121-132.
Howell, B. W., Hawkes, R., Soriano, P. and Cooper, J. A. (1997b). Neuronal position in the developing brain is regulated by mouse disabled-1. *Nature* **389**, 733-737.
Kiehart, D. P., Galbraith, C. G., Edwards, K. A., Rickoll, W. L. and Montague, R. A. (2000). Multiple forces contribute to cell sheet morphogenesis for dorsal closure in Drosophila. *J. Cell. Biol.* **149**, 471-490.
Koleske, A. J., Gifford, A. M., Scott, M. L., Nee, M., Bronson, R. T., Miczek, K. A. and Baltimore, D. (1998). Essential roles for the Abl and Arg tyrosine kinases in neurulation. *Neuron* **21**, 1259-1272.
Le, N. and Simon, M. A. (1998). Disabled is a putative adaptor protein that functions during signaling by the sevenless receptor tyrosine kinase. *Mol. Cell. Biol.* **18**, 4844-4854.
Le Gall, M. and Giniger, E. (2004). Identification of two binding regions for the suppressor of hairless protein within the intracellular domain of Drosophila notch. *J. Biol. Chem.* **279**, 29418-29426.
Le Gall, M., De Mattei, C. and Giniger, E. (2008). Molecular separation of two signaling pathways for the receptor, Notch. *Dev. Biol.* **313**, 556-567.
Liebl, E. C., Forsthoefel, D. J., Franco, L. S., Sample, S. H., Hess, J. E., Cowger, J. A., Chandler, M. P., Shupert, A. M. and Seeger, M. A. (2000). Dosage-sensitive, reciprocal genetic interactions between the Abl tyrosine kinase and the putative GEF trio reveal trio's role in axon pathfinding. *Neuron* **26**, 107-118.
Liebl, E. C., Rowe, R. G., Forsthoefel, D. J., Stammler, A. L., Schmidt, E. R., Turski, M. and Seeger, M. A. (2003). Interactions between the secreted protein Amalgam, its transmembrane receptor Neurotactin and the Abelson tyrosine kinase affect axon pathfinding. *Development* **130**, 3217-3226.
Lin, T. Y., Huang, C. H., Kao, H. H., Liou, G. G., Yeh, S. R., Cheng, C. M., Chen, M. H., Pan, R. L. and Juang, J. L. (2009). Abi plays an opposing role to Abl in Drosophila axonogenesis and synaptogenesis. *Development* **136**, 3099-3107.
Moresco, E. M. and Koleske, A. J. (2003). Regulation of neuronal morphogenesis and synaptic function by Abl family kinases. *Curr. Opin. Neurobiol.* **13**, 535-544.
Moresco, E. M., Donaldson, S., Williamson, A. and Koleske, A. J. (2005). Integrin-mediated dendrite branch maintenance requires Abelson (Abl) family kinases. *J. Neurosci.* **25**, 6105-6118.
Parks, S. and Wieschaus, E. (1991). The Drosophila gastrulation gene concertina encodes a G alpha-like protein. *Cell* **64**, 447-458.
Pendergast, A. M. (2002). The Abl family kinases: mechanisms of regulation and signaling. *Adv. Cancer Res.* **85**, 51-100.
Sibbe, M., Forster, E., Basak, O., Taylor, V. and Frotscher, M. (2009). Reelin and Notch1 cooperate in the development of the dentate gyrus. *J. Neurosci.* **29**, 8578-8585.
Stevens, T. L., Rogers, E. M., Koontz, L. M., Fox, D. T., Homem, C. C., Nowotarski, S. H., Artabazon, N. B. and Peifer, M. (2008). Using Bcr-Abl to examine mechanisms by which abl kinase regulates morphogenesis in Drosophila. *Mol. Biol. Cell* **19**, 378-393.
Wills, Z., Bateman, J., Korey, C. A., Comer, A. and Van Vactor, D. (1999a). The tyrosine kinase Abl and its substrate enabled collaborate with the receptor phosphatase Dlar to control motor axon guidance. *Neuron* **22**, 301-312.
Wills, Z., Marr, L., Zinn, K., Goodman, C. S. and Van Vactor, D. (1999b). Profilin and the Abl tyrosine kinase are required for motor axon outgrowth in the Drosophila embryo. *Neuron* **22**, 291-299.
Wills, Z., Emerson, M., Rusch, J., Bikoff, J., Baum, B., Perrimon, N. and Van Vactor, D. (2002). A Drosophila homolog of cyclase-associated proteins collaborates with the Abl tyrosine kinase to control midline axon pathfinding. *Neuron* **36**, 611-622.